Kinetic Studies of the Reactions of O 2 (b 1 Σ g +) with Several Atmospheric Molecules

ARTICLE *in* THE JOURNAL OF PHYSICAL CHEMISTRY A · MAY 2005

Impact Factor: 2.69 · DOI: 10.1021/jp044129x · Source: PubMed

3 AUTHORS:

Edward Dunlea
National Academies
82 PUBLICATIONS **3,405** CITATIONS
SEE PROFILE

Ranajit K Talukdar
National Oceanic and Atmospheric Administr…
104 PUBLICATIONS **2,772** CITATIONS
SEE PROFILE

A.R. Ravishankara
Colorado State University
508 PUBLICATIONS **18,473** CITATIONS
SEE PROFILE

Kinetic Studies of the Reactions of $O_2(b^1\Sigma_g^+)$ with Several Atmospheric Molecules

Edward J. Dunlea, Ranajit K. Talukdar, and A. R. Ravishankara*

Aeronomy Laboratory, National Oceanic and Atmospheric Administration, 325 Broadway, Boulder, Colorado 80305, and Cooperative Institute for Research in Environmental Sciences and the Department of Chemistry and Biochemistry, University of Colorado, Boulder, Colorado 80309

Received: December 24, 2004; In Final Form: March 2, 2005

Thermal rate coefficients for the removal (reaction + quenching) of $O_2(^1\Sigma_g^+)$ by collision with several atmospheric molecules were determined to be as follows: O_3, $k_3(210-370\ K) = (3.63 \pm 0.86) \times 10^{-11} \exp((-115 \pm 66)/T)$; H_2O, $k_4(250-370\ K) = (4.52 \pm 2.14) \times 10^{-12} \exp((89 \pm 210)/T)$; N_2, $k_5(210-370\ K) = (2.03 \pm 0.30) \times 10^{-15} \exp((37 \pm 40)/T)$; CO_2, $k_6(298\ K) = (3.39 \pm 0.36) \times 10^{-13}$; CH_4, $k_7(298\ K) = (1.08 \pm 0.11) \times 10^{-13}$; CO, $k_8(298\ K) = (3.74 \pm 0.87) \times 10^{-15}$; all units in cm^3 $molecule^{-1}$ s^{-1}. $O_2(^1\Sigma_g^+)$ was produced by directly exciting ground-state $O_2(^3\Sigma_g^-)$ with a 762 nm pulsed dye laser. The reaction of $O_2(^1\Sigma_g^+)$ with O_3 was used to produce $O(^3P)$, and temporal profiles of $O(^3P)$ were measured using VUV atomic resonance fluorescence in the presence of the reactant to determine the rate coefficients for removal of $O_2(^1\Sigma_g^+)$. Our results are compared with previous values, where available, and the overall trend in the $O_2(^1\Sigma_g^+)$ removal rate coefficients and the atmospheric implications of these rate coefficients are discussed. Additionally, an upper limit for the branching ratio of $O_2(^1\Sigma_g^+) + CO$ to give $O(^3P) + CO_2$ was determined to be $\leq 0.2\%$ and this reaction channel is shown to be of negligible importance in the atmosphere.

Introduction

The reactions of the second electronically excited state of molecular oxygen, $O_2(b^1\Sigma_g^+)$ (hereafter referred to as $O_2(^1\Sigma_g^+)$), have been studied in the past for a variety of reasons including their involvement in terrestrial airglow and chemical lasers (see Wayne, 1985,[1] and Schweitzer and Schmidt, 2003,[2] for reviews). In addition, it has been proposed that $O_2(^1\Sigma_g^+)$ may influence the chemistry of the stratosphere and upper troposphere significantly as a source of odd-hydrogen (HO_x) or odd-nitrogen (NO_x).[3−5] It is this last reason that motivated two recent studies in our laboratory.[6,7]

To assess the potential influence of $O_2(^1\Sigma_g^+)$ on the atmosphere, one needs the atmospheric concentration of $O_2(^1\Sigma_g^+)$; concentrations are determined by the balance of the rates of the production and loss of $O_2(^1\Sigma_g^+)$. Atmospheric $O_2(^1\Sigma_g^+)$ is produced either via direct absorption of visible radiation near 762 nm or collisional deactivation of electronically excited oxygen atoms, $O(^1D)$, by ground-state molecular oxygen, $O_2(^3\Sigma_g^-)$.

$$O_2(^3\Sigma_g^-) + h\nu\ (\sim 762\ nm) \rightarrow O_2(^1\Sigma_g^+) \quad (1)$$

$$O(^1D) + O_2(^3\Sigma_g^-) \rightarrow O(^3P) + O_2(^1\Sigma_g^+) \quad (2)$$

The atmospheric $O_2(^1\Sigma_g^+)$ production rate therefore depends on the visible and ultraviolet actinic flux,[8] the pressure dependent line shapes of the $O_2(^1\Sigma_g^+) \leftarrow O_2(^3\Sigma_g^-)$ transitions,[9] the absorption cross sections for O_3 to produce $O(^1D)$,[10] the rate coefficient for quenching of $O(^1D)$ by $O_2(^3\Sigma_g^-)$,[11−15] and the abundances of O_2 and O_3.

The primary loss of $O_2(^1\Sigma_g^+)$ in the atmosphere is believed to be via electronic quenching to $O_2(^1\Delta_g)$ by other atmospheric gases.[1] While there have been many previous measurements of the rate coefficients of $O_2(^1\Sigma_g^+)$ with a variety of atmospheric molecules,[1,10] there are significant uncertainties in the reported values, and in some cases, there is no information on the temperature dependences of the rate coefficients. Furthermore, almost all previous measurements have employed similar methods for their studies by observing the rate of loss of $O_2(^1\Sigma_g^+)$. Studies using a different method are therefore helpful in reducing the overall uncertainty in the rate coefficient values.

In this study, we measured the rate coefficients for $O_2(^1\Sigma_g^+)$ removal by a number of atmospheric gases at atmospherically relevant temperatures.

$$O_2(^1\Sigma_g^+) + O_3 \rightarrow \text{products} \quad (3)$$

$$O_2(^1\Sigma_g^+) + H_2O \rightarrow \text{products} \quad (4)$$

$$O_2(^1\Sigma_g^+) + N_2 \rightarrow \text{products} \quad (5)$$

$$O_2(^1\Sigma_g^+) + CO_2 \rightarrow \text{products} \quad (6)$$

$$O_2(^1\Sigma_g^+) + CH_4 \rightarrow \text{products} \quad (7)$$

$$O_2(^1\Sigma_g^+) + CO \rightarrow \text{products} \quad (8)$$

At atmospherically relevant temperatures, the only thermodynamically possible pathway is the quenching of $O_2(^1\Sigma_g^+)$ to either $O_2(^1\Delta_g)$ or $O_2(^3\Sigma_g^-)$ in most reactions. However, the reactions of $O_2(^1\Sigma_g^+)$ with O_3 can lead to $2O_2$ and $O(^3P)$, and that with CO can lead to CO_2 and $O(^3P)$.

* To whom correspondence should be addressed at the National Oceanic and Atmospheric Administration.

10.1021/jp044129x CCC: $30.25
Published on Web 04/12/2005

$$O_2(^1\Sigma_g^+) + O_3 \rightarrow 2\,O_2 + O(^3P); \quad \Delta_{rxn}H_{298} = -12.0 \text{ kcal/mol} \quad (3a)$$

$$O_2(^1\Sigma_g^+) + O_3 \rightarrow O_2(^1\Delta_g)\{O_2(^3\Sigma_g^-)\} + O_3; \quad \Delta_{rxn}H_{298} = -15.0\{-37.5\} \text{ kcal/mol} \quad (3b)$$

$$O_2(^1\Sigma_g^+) + CO \rightarrow O(^3P) + CO_2; \quad \Delta_{rxn}H_{298} = -45.6 \text{ kcal/mol} \quad (8a)$$

$$O_2(^1\Sigma_g^+) + CO \rightarrow O_2(^1\Delta_g)\{O_2(^3\Sigma_g^-)\} + CO; \quad \Delta_{rxn}H_{298} = -15.0\{-37.5\} \text{ kcal/mol} \quad (8b)$$

The yield of $O(^3P)$ in reaction 3 has been previously reported to be between 0.75 and 1.[16,17] We measured the upper limits for the yields of $O(^3P)$ and of CO_2 from reaction 8a to determine whether this reaction has any atmospheric significance.

Experiments

Pulsed Photolysis. Resonance Fluorescence Detection of $O(^3P)$. Our experiments utilized pulsed generation of $O_2(^1\Sigma_g^+)$ via excitation and $O(^3P)$ detection via resonance fluorescence (PP−RF) in the vacuum ultraviolet (VUV); this apparatus has been described in detail elsewhere.[15,18,19] We emphasize that we did not directly measure the temporal profiles of $O_2(^1\Sigma_g^+)$. Instead, $O(^3P)$ atoms produced via the reaction of $O_2(^1\Sigma_g^+)$ with O_3 (reaction 3a) were monitored. $O_2(^1\Sigma_g^+)$ was produced via reaction 1 with a tunable dye laser in the presence of an excess of stable reactant gases ($([X]/[O_2(^1\Sigma_g^+)]_0) > 30$) such that $O_2(^1\Sigma_g^+)$ loss was first order in its concentration. The photolysis laser was tuned to the peak of the individual $O_2(^1\Sigma_g^+) \leftarrow O_2(^3\Sigma_g^-)$ transitions by monitoring the photoacoustic signal from 100 Torr of O_2 in a separate absorption cell.[6] Temporal profiles of $O(^3P)$ following $O_2(^1\Sigma_g^+)$ generation were measured in the presence of a range of concentrations of the stable reactant to determine the overall rate coefficient for removal of $O_2(^1\Sigma_g^+)$ by that reactant. The first-order rate coefficient for the rise in $O(^3P)$ signal was equivalent to the first-order rate coefficient for $O_2(^1\Sigma_g^+)$ loss; so the kinetic information on $O_2(^1\Sigma_g^+)$ was obtained from the $O(^3P)$ temporal profiles. This method determines the rate coefficient for the sum of quenching and reaction of $O_2(^1\Sigma_g^+)$. Experimental conditions used for measuring k_3 through k_8 are listed in Table 1. Reactions 6−8 were studied only at room temperature, reactions 3 and 5 were studied between 210 and 370 K, and reaction 4 was investigated between 250 and 370 K.

The initial concentrations of $O_2(^1\Sigma_g^+)$ were estimated from the laser fluence and absorption line strengths for the $O_2(^1\Sigma_g^+) \leftarrow O_2(^3\Sigma_g^-)$ transition as described in Talukdar et al.[6] The absorption of radiation near 762 nm by $O_2(^3\Sigma_g^-)$ occurs over very narrow wavelength ranges and the dye laser must be carefully tuned to maximize the production of $O_2(^1\Sigma_g^+)$. The concentrations of $O(^3P)$ were estimated from the calculated initial $O_2(^1\Sigma_g^+)$ concentrations, assuming that reaction 3 produced at most one $O(^3P)$, and by taking into account the loss of $O_2(^1\Sigma_g^+)$ via reactions other than reaction 3. Maintaining a sufficiently low $O(^3P)$ concentration ($<10^{12}$ molecules cm^{-3}) minimized regeneration of $O_2(^1\Sigma_g^+)$ via the $O(^3P)$ self-reaction.

$$O(^3P) + O(^3P) + M \rightarrow O_2(^1\Sigma_g^+) + M \quad (9)$$

Reaction 9 has been known to produce $O_2(^1\Sigma_g^+)$ in some previous studies[20] where a microwave discharge source for $O_2(^1\Sigma_g^+)$ was used. In our experiments, $O_2(^1\Sigma_g^+)$ generation from reaction 9 was insignificant ($k_9 \sim 2 \times 10^{-33}$ cm^6 $molecule^{-2}$ s^{-1},[21] which yields $k_9(\text{bimolecular}) = 5 \times 10^{-15}$ at 80 Torr and leads to a negligible (<0.1%) loss of $O(^3P)$ due to this reaction in 100 ms). $O_2(^1\Delta_g)$ produced by the quenching of $O_2(^1\Sigma_g^+)$ was therefore also in sufficiently low concentrations that the energy pooling reaction of $O_2(^1\Delta_g)$ with itself would not regenerate significant amounts of $O_2(^1\Sigma_g^+)$.

$$O_2(^1\Delta_g) + O_2(^1\Delta_g) \rightarrow O_2(^1\Sigma_g^+) + O_2(^3\Sigma_g^-) \quad (10)$$

Last, the lack of $O(^3P)$ signal when O_3 was absent or when the laser was not tuned to the peak of an $O_2(^1\Sigma_g^+) \leftarrow O_2(^3\Sigma_g^-)$ transition showed that there were no other $O(^3P)$ production processes and that the photolysis of O_3 by 762 nm radiation did not produce significant concentrations of $O(^3P)$.

The excess reactants were prepared and their concentrations determined via several different methods. Ozone was subjected to several freeze-pump-thaw cycles (at 97 K) to remove O_2 prior to making dilute mixtures in He (~1%) in 12 L Pyrex bulbs. During all rate coefficient measurements, the O_3 concentration in the gas stream flowing through the reactor was determined by measuring the absorption of 253.7 nm light ($\sigma = 1.15 \times 10^{-17}$ cm^2)[10] in a 100 cm long cell. The uncertainty in determining the O_3 concentration, due to variation in the intensity of the light source, was estimated to be $<\pm 2\%$. The method for preparing a stable flow of water vapor and measuring its concentration has been described in detail elsewhere.[22] Briefly, we bubbled a small flow (0−100 sccm) of He through distilled liquid H_2O maintained at 273 K (by immersing the bubbler in an ice/water bath) and metered out a small flow of this moist He through a needle valve. The water vapor concentration was determined by measuring the absorption of 121.6 nm light ($\sigma = (1.59 \pm 0.10) \times 10^{-17}$ cm^2)[23,24] in a 19 cm cell prior to the reactor. The following gases (with the vendor and purity level indicated within parentheses) were used in these experiments without further purification: UHP He (US Welding, > 99.999%), UHP O_2 (Scott Specialty Gases, >99.99%), UHP N_2 (Scott Specialty Gases, >99.9995%), UHP CO_2 (Scott Specialty Gases, >99.99%), UHP CO (Spectra Gases, >99.99%), and UHP CH_4 (Scientific Gas Products, >99.97%). Concentrations of these stable gases in the reactor were calculated using the mass flow rates (measured using calibrated electronic mass flow meters) and pressures (measured using capacitance manometers). The uncertainties in the mass flow rate and pressure measurements were all ± 2%, leading to uncertainties of at most ± 10% (2σ) for the concentration of the stable gases in the reactor.

FTIR Detection of CO_2. A Fourier transform infrared spectrometer (FTIR) was employed to search for CO_2 produced from reaction 8a. The CO_2 concentration was calculated using Beer's law by comparing the spectrum recorded with an evacuated cell to that filled with the reaction products, and using the known integrated line strength for the entire absorption feature of the CO_2 stretch near 2350 cm^{-1} ($\sigma = 1.01 \times 10^{-16}$ cm^2 cm^{-1}) (from the HITRAN database[9]). Using the integrated line strength for the absorption feature (in cm^2 cm^{-1}) avoids corrections for pressure and Doppler broadening of individual rotational lines.

These experiments involved detecting the possible production of CO_2 from reaction 8 in the presence of CO. Figure 1a displays the absorption spectrum of a mixture of $CO/CO_2/O_2$ and shows that the CO_2 absorption feature at 2350 cm^{-1} and the CO stretch near 2140 cm^{-1} ($\sigma = 1.01 \times 10^{-17}$ cm^2 cm^{-1} [9]) do not overlap. Known mixtures of CO_2/O_2 and $CO/CO_2/O_2$ were prepared in

TABLE 1: Rate Coefficients for the Removal of $O_2(^1\Sigma_g^+)$ by Various Molecules and the Experimental Conditions Used to Measure Them

molecule	temp (K)	overall pressure (Torr)	$[O_3]$ (10^{13} molecule cm^{-3})	$[O_2]$ (10^{17} molecule cm^{-3})	762 nm fluence (mJ $pulse^{-1}$)	$[O_2(^1\Sigma_g^+)]_0$ (10^{11} molecule cm^{-3})	range of excess reactant concn (molecule cm^{-3})	k' range (s^{-1})	rate coeff (cm^3 $molecule^{-1}$ s^{-1})
O_3	210	20	2.95−27.9	1.79	8	8.1		730−5940	$(2.03 \pm 0.10) \times 10^{-11}$
	232	18	3.15−53.1	2.5	3	3.6		740−12180	$(2.20 \pm 0.14) \times 10^{-11}$
	248	18	4.38−47.5	2.3	3.5	3.6		1030−12000	$(2.24 \pm 0.20) \times 10^{-11}$
	268	18	1.96−45.4	2.1	3	2.7		730−11300	$(2.24 \pm 0.03) \times 10^{-11}$
	295	16.7	1.69−24.5	1.36	4	2.3−6.4		440−5830	$(2.36 \pm 0.11) \times 10^{-11}$
	321	18.5	2.21−45.6	1.85	4	2.8		720−10480	$(2.34 \pm 0.14) \times 10^{-11}$
	348	18.5	1.47−39.6	1.75	4	2.5		580−10490	$(2.58 \pm 0.22) \times 10^{-11}$
	373	18.8	3.72−35.0	1.6	3.5	1.9		1200−10050	$(2.89 \pm 0.14) \times 10^{-11}$
H_2O	248	18	4	2.22	2.6−7	2.7−7.3	$(7.74-18.1) \times 10^{14}$	860−13880	$(6.59 \pm 0.20) \times 10^{-12}$
	268	18	2.5	2.1	2.7−6.2	2.5−5.7	$(5.77-17.4) \times 10^{14}$	550−10440	$(6.45 \pm 0.43) \times 10^{-12}$
	295	18.5	2.0−2.5	1.73−1.95	1.3−7	0.9−5.6	$(1.61-15.3) \times 10^{14}$	680−8700	$(5.41 \pm 0.54) \times 10^{-12}$
	348	18.5	2.2	1.69	3.8−8.5	2.3−5.2	$(4.89-17.4) \times 10^{14}$	750−11200	$(5.63 \pm 0.43) \times 10^{-12}$
	373	18.5	4	1.56	3.3−8	1.8−4.3	$(2.71-16.3) \times 10^{14}$	1060−10570	$(5.64 \pm 0.76) \times 10^{-12}$
N_2	210	80	15	1.83	6	6.1	$(1.61-29.3) \times 10^{17}$	2870−9390	$(2.38 \pm 0.28) \times 10^{-15}$
	230	80	11	1.96	8	8.5	$(1.15-27.5) \times 10^{17}$	2250−8550	$(2.34 \pm 0.20) \times 10^{-15}$
	250	80	13	1.73	8	7.2	$(1.10-25.5) \times 10^{17}$	2730−9850	$(2.44 \pm 0.14) \times 10^{-15}$
	273	80	12	1.7	8	6.8	$(1.17-22.6) \times 10^{17}$	2660−8430	$(2.44 \pm 0.36) \times 10^{-15}$
	295	80.5	10	1.80	6	5.2	$(1.42-24.5) \times 10^{17}$	2432−8210	$(2.23 \pm 0.11) \times 10^{-15}$
	323	82	8	1.68	4−8	3.2−6.4	$(2.28-21.1) \times 10^{17}$	1870−6550	$(2.21 \pm 0.14) \times 10^{-15}$
	350	81	7	1.56	8.5	6.2	$(1.91-19.5) \times 10^{17}$	1690−5980	$(2.18 \pm 0.17) \times 10^{-15}$
	373	80	7	1.61	8	5.5	$(0.84-16.7) \times 10^{17}$	1780−5600	$(2.31 \pm 0.22) \times 10^{-15}$
CO_2	295	25	7.50	1.81	5−10	4.3−8.6	$(8.5-104) \times 10^{14}$	1840−6690	$(3.39 \pm 0.20) \times 10^{-13}$
CH_4	295	25.2	1.40	1.81	5−23	4.3−19.9	$(1.32-16.8) \times 10^{16}$	390−2233	$(1.08 \pm 0.70) \times 10^{-13}$
CO	295	71.5	8.10	1.80	4−10	3.4−8.6	$3.8-182 \times 10^{16}$	1940−9690	$(3.74 \pm 0.44) \times 10^{-15}$

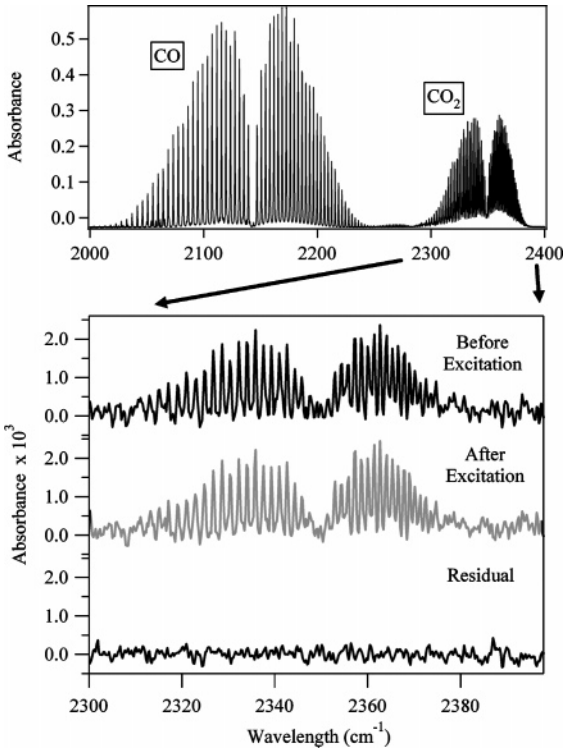

Figure 1. (a, top panel) FTIR absorption features for CO and CO_2 measured with spectrometer resolution of 0.5 cm^{-1} ($[CO_2] = 4.5 \times 10^{16}$ molecules cm^{-3} and $[CO] = 9.0 \times 10^{17}$ molecules cm^{-3}). (b; bottom panel). FTIR absorption feature for CO_2 seen before and after the production of $O_2(^1\Sigma_g^+)$ to determine an upper limit of CO_2 production from the $O_2(^1\Sigma_g^+)$ + CO reaction. The two features and the residual between them have all been offset for clarity. The residual shows no indication of CO_2 production, suggesting a negligible production of CO_2 due to reaction 8a.

a 40 cm long (2 cm diameter) photolysis cell, then expanded into a 10 cm cell placed in the optical path of the FTIR spectrometer. This method minimized the interference from ambient CO_2 within the FTIR. The agreement for concentrations determined spectroscopically with those determined manometrically was within a factor of 2 for CO_2 and was within a factor of 3 for CO. These differences were most probably limited by the resolution of the FTIR (0.5 cm^{-1}), and since we determine only upper limits for the CO_2 concentrations (see later discussion), we did not spend too much effort in resolving the discrepancy between the Beer's law/HITRAN calculation and the manometrically prepared mixtures. Overall, CO_2 concentrations as low as 1×10^{14} molecules cm^{-3} were detectable in the photolysis cell.

Results

Rate Coefficient Measurements. The method employed to analyze data on rate coefficients reported here was the same as that used in the $O(^1D)$ reaction studies described in Dunlea and Ravishankara.[15] The temporal profiles of $O(^3P)$ measured here were described by a biexponential function:

$$[O(^3P)]_t = Ae^{-Bt} + Ce^{-Dt} \quad \text{(I)}$$

Using the reaction of $O_2(^1\Sigma_g^+) + N_2$ as an example, parameters *A*, *B*, *C*, and *D* are defined as follows:

$$A = [O_2(^1\Sigma_g^+)]_0 \frac{(k_3[O_3] + k_5[N_2])}{(D - B)} \quad \text{(II)}$$

$$B = k_3[O_3] + k_5[N_2] + k_{12} \quad \text{(III)}$$

$$C = [O(^3P)]_0 - A \quad \text{(IV)}$$

$$D = k_{11} \quad \text{(V)}$$

k_{11} and k_{12} are, respectively, the rate coefficient for the first-order loss of $O(^3P)$ due to flow out of the reaction zone, and the rate coefficient for the first-order loss of $O_2(^1\Sigma_g^+)$ due to both flow and quenching by the bath gas.

$$O(^3P) \rightarrow \text{loss} \quad (11)$$

$$O_2(^1\Sigma_g^+) \rightarrow \text{loss} \quad (12)$$

The sum of the parameters $A + C$ was equal to the initial concentration of $O(^3P)$, $[O(^3P)]_0$, produced via the photolysis of O_3 in the Chappuis band at 762 nm. It was very small compared to the total $O(^3P)$ signal from the $O_2(^1\Sigma_g^+) + O_3$ reaction as mentioned above.

Figure 2 shows the measured first-order rate coefficient at 298 K for the $O(^3P)$ rise (the B parameter in eq III) plotted against the reactant concentration; the slope of each line is the bimolecular rate coefficient for the removal of $O_2(^1\Sigma_g^+)$ by that reactant via both reaction and quenching. The determined rate coefficients are also listed in Table 1. Uncertainties in the rate coefficients are reported at the 2σ level and were derived from the uncertainty in the reactant concentration, the uncertainty in the fit of the $O(^3P)$ temporal profile to eq III ($\pm 3\%$ [15]) and the uncertainty in the slope obtained in the linear least-squares fit of the *B* parameter vs the reactant concentration, all summed in quadrature.

The intercept of the plot of the *B* parameter vs $[O_3]$ (top panel of Figure 2) represents k_{12}, the first-order rate coefficient for the background loss of $O_2(^1\Sigma_g^+)$. This loss rate coefficient is the sum of those for $O_2(^1\Sigma_g^+)$ loss via quenching by O_2 and He and the loss due to loss of $O_2(^1\Sigma_g^+)$ out of the detection region (assumed to be first order):

$$O_2(^1\Sigma_g^+) + O_2 \rightarrow \text{products} \quad (13)$$

$$O_2(^1\Sigma_g^+) + He \rightarrow \text{products} \quad (14)$$

$$O_2(^1\Sigma_g^+) \rightarrow \text{loss due to flow out of detection region} \quad (15)$$

Ascribing the measured $O_2(^1\Sigma_g^+)$ loss rate coefficient only to reactions 13 and 14 and using a literature value[25] for k_{14} of 2.5×10^{-16} cm^3 molecule^{-1} s^{-1} yields an upper limit for k_{13} of $< 1 \times 10^{-15}$ cm^3 molecule^{-1} s^{-1} at room temperature.

Large concentrations of CH_4 were necessary to observe a change in the measured loss rate of $O_2(^1\Sigma_g^+)$ (Figure 2, middle panel) due to reaction 7. CH_4 absorbs the VUV radiation used for $O(^3P)$ detection ($\sigma_{131\text{ nm}}(CH_4) \sim 2 \times 10^{-17}$ cm^2 [26]). Therefore, the range of first-order rate coefficients for loss of $O_2(^1\Sigma_g^+)$ was restricted to small values and thus yielded a less precise value of k_7.

Figure 3 shows the rate coefficients, k_3 and k_5, measured between 210 and 370 K, and k_4, measured between 250 and 370 K, in an Arrhenius form. These data were fit to the expression

$$\ln(k) = \ln(A) - \frac{E_a}{(RT)} \quad \text{(VI)}$$

using an unweighted linear least-squares method. The uncertainty in the Arrhenius preexponential factor is defined as $\sigma_A = A\sigma_{\ln A}$. The obtained values are listed in Tables 2−4.

Upper Limit for $O(^3P)$ Production from $O_2(^1\Sigma_g^+) + CO$. Using the RF detection of $O(^3P)$, we ran a pair of back-to-back experiments to determine an upper limit for the yield of $O(^3P)$ from channel 8a. The first run involved the excitation of an $O_2(^1\Sigma_g^+) \leftarrow O_2(^3\Sigma_g^-)$ transition in a flowing mixture of O_2, O_3, He, and CO. Then the same experiment was repeated in the absence of O_3. In the first run, reaction 3 was responsible for producing a known amount of $O(^3P)$ with the possible addition of $O(^3P)$ from reaction 8a. In the second run, only reaction 8a could have produced $O(^3P)$. As can be seen in Figure 4, there was no measurable production of $O(^3P)$ from reaction 8a. The $O(^3P)$ concentration was calculated as described previously,[6] and was varied in the range $(0.37-1.69) \times 10^{11}$ molecules cm^{-3}. The CO concentrations were such ($\sim 2 \times 10^{18}$ molecules cm^{-3}) that more than 65% of the $O_2(^1\Sigma_g^+)$ molecules were lost via deactivation by CO. The rest of the $O_2(^1\Sigma_g^+)$ reacted with O_3 ($(7-9) \times 10^{13}$ molecules cm^{-3}). The rise in the $O(^3P)$ signal due to the $O_2(^1\Sigma_g^+) + O_3$ reaction was completed (>99%) within the first 300 μs and the $O(^3P)$ temporal profiles were fit to a single-exponential decay for times >300 μs to determine the signal associated with the $[O(^3P)]_0$. The maximum possible $O(^3P)$ concentration produced in the second run was determined from twice the standard deviation of the background signal of the second run multiplied by the ratio of the known $[O(^3P)]_0$ in the first run. Dividing this maximum possible $O(^3P)$ concentration by the $O_2(^1\Sigma_g^+)$ concentration gives an upper limit for the yield of $O(^3P)$ production from reaction 8a. In two separate determinations, upper limits for this yield were determined to be 0.01 and 0.06; therefore, we report an upper limit for the production of $O(^3P)$ from reaction 8a of 0.06.

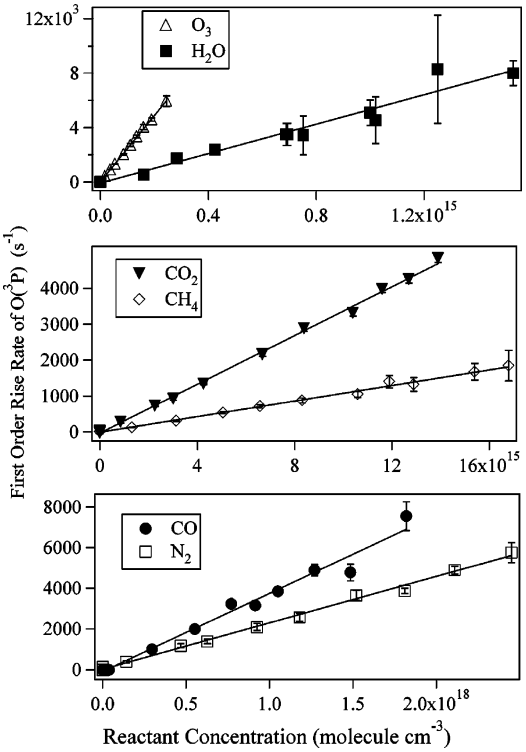

Figure 2. Plots of the first-order $O(^3P)$ rise rate coefficients (the *B* parameter from eq III described in text) vs the concentration of stable reactant for $O_2(^1\Sigma_g^+)$ reactions at 295 K. The slope of each fitted line is the room-temperature bimolecular rate coefficients for removal of $O_2(^1\Sigma_g^+)$. In the top panel, the intercept of the plot for reaction 3 was used to determine an upper limit for the rate coefficient for the quenching of $O_2(^1\Sigma_g^+)$ by O_2 (see text). For all other reactions, the loss of $O_2(^1\Sigma_g^+)$ in the absence of reactant has been accounted for in the plotted rise rate coefficients; thus all other intercepts are zero.

Upper Limit for CO_2 Production from $O_2(^1\Sigma_g^+) + CO$. For measuring the CO_2 yield in reaction 8, we generated $O_2(^1\Sigma_g^+)$ in the presence of CO and measured any CO_2 produced via reaction 8a by FTIR spectroscopy. Owing to the significant concentration of CO_2 required for detection with the FTIR and the small yield of CO_2 inferred from the low $O(^3P)$ yield (described in previous section), we produced a large concentration of $O_2(^1\Sigma_g^+)$ in a static mixture to enhance detectable production of CO_2. Since CO_2 is stable and its reactivity with

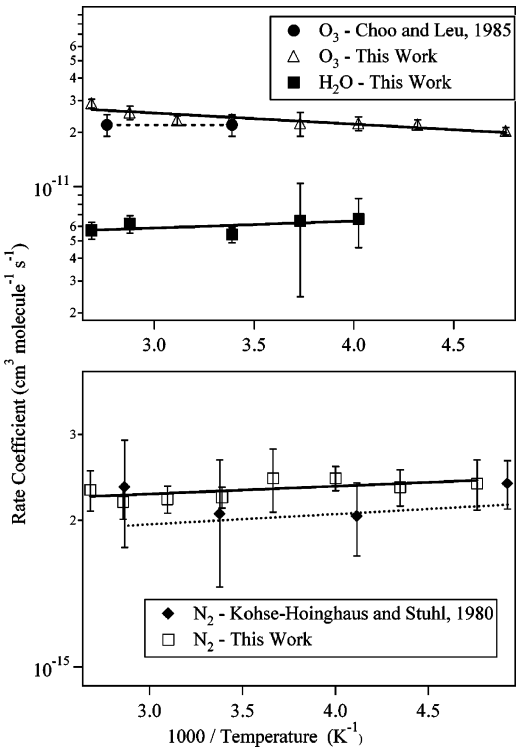

Figure 3. Measured rate coefficients for the overall removal of $O_2(^1\Sigma_g^+)$ by O_3 and H_2O (top panel) and by N_2 (bottom panel) displayed vs 1000/*T*. Fits to the Arrhenius expression, eq VI, are shown: dashed lines indicate fits in previous studies, solid lines indicate fits in present study. The Arrhenius parameters determined from these fits are listed in Tables 2−4.

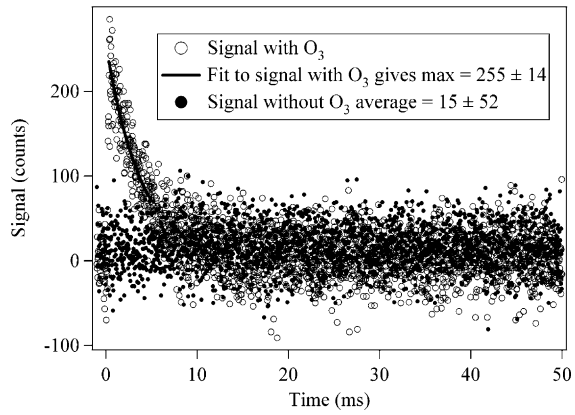

Figure 4. Temporal profiles of $O(^3P)$ signal recorded back-to-back for the 762 nm excitation of a mixture of $CO/O_3/O_2$ followed by a mixture of CO/O_2 used to search for $O(^3P)$ production from $O_2(^1\Sigma_g^+)$ + CO. No visible production of $O(^3P)$ was observed in the second run (solid circles in figure) due to reaction 8a.

$O_2(^1\Sigma_g^+)$ or $O(^3P)$ is very small, one would not expect any removal of CO_2 in this system. We systematically tested this by irradiating mixtures containing known amounts of CO_2 in O_2 with the 762 nm laser tuned to an $O_2(^1\Sigma_g^+) \leftarrow O_2(^3\Sigma_g^-)$ transition to determine whether CO_2 was lost during the photolysis process. Mixtures were prepared at total pressures of approximately 700 Torr and expanded into an absorption cell placed in the optical path of the FTIR spectrometer for analysis before and after the photolysis. The CO_2/O_2 gas mixtures were exposed to $>2 \times 10^4$ laser pulses at 762 nm to produce as much as 4.4×10^{16} molecules cm^{-3} of $O_2(^1\Sigma_g^+)$. The CO_2 concentrations after photolysis in several of these CO_2/O_2 mixtures were unchanged (<10% differences and limited by our precision). The same was true for both the CO_2 and CO concentrations in all $CO_2/CO/O_2$ mixtures tested. Slight changes, if any, were within the precision of our measurement. This sequence of experiments showed that CO_2 was not lost in the cell due to either reaction with $O_2(^1\Sigma_g^+)$ or with any species produced by the quenching of $O_2(^1\Sigma_g^+)$ by CO or O_2.

For the final experiment, a CO/O_2 mixture was irradiated with $> 5.5 \times 10^4$ pulses from the 762 nm laser to produce 5.6×10^{16} molecules cm^{-3} of $O_2(^1\Sigma_g^+)$. Figure 1b shows the small, and unavoidable, CO_2 absorption feature present due to small amounts of air within the FTIR both before and after the photolysis. The residual between the two shows no structure resembling CO_2, confirming that reaction 8a did not produce CO_2 within our detection limits. We determine an upper limit for the yield of channel 8a from twice the standard deviation of the residual spectrum over the 60 cm^{-1} range in which the feature was present and the total $O_2(^1\Sigma_g^+)$ concentration. Our upper limit is $<1.2 \times 10^{-3}$ for the yield of CO_2 in the reaction of $O_2(^1\Sigma_g^+)$ with CO.

Discussion

In this section, our results for the individual $O_2(^1\Sigma_g^+)$ reaction rate coefficients are compared with those from previous studies. The majority of these previous studies have monitored the time-resolved fluorescence of the $O_2(^1\Sigma_g^+) \rightarrow O_2(^3\Sigma_g^-)$ transition near 762 nm.[27] The uncertainty in the rate coefficients reported from these studies depended (to a great extent) on the method used for generation of $O_2(^1\Sigma_g^+)$. There have been three major sources of $O_2(^1\Sigma_g^+)$: discharge flow, which employed a microwave discharge plasma containing O_2,[20,28−35] flash photolysis of O_2 or O_3 to produce $O(^1D)$, which was then quenched by O_2 to produce $O_2(^1\Sigma_g^+)$,[12,25,36−45] and direct excitation of $O_2(^1\Sigma_g^+) \leftarrow O_2(^3\Sigma_g^-)$ with a dye laser.[46−49]

Many early discharge flow studies,[27,30] including those employing shock tubes to reach higher temperatures,[50−52] suffered from interferences due to secondary production of $O_2(^1\Sigma_g^+)$ from $O(^3P)$ atom recombination (reaction 9). Secondary production of $O_2(^1\Sigma_g^+)$ would have led to the measured decay rates of $O_2(^1\Sigma_g^+)$ being slower than real and yielding smaller values of rate coefficients. Flash photolysis studies were also prone to interferences from secondary reactions, including reactions 9 and 10. Therefore, flash photolysis studies, which produced $O_2(^1\Delta_g)$ generally needed to maintain low radical concentrations, often limiting signal levels. Direct excitation studies require large laser fluences to produce detectable amounts of $O_2(^1\Sigma_g^+)$ owing to the small line strengths of the $O_2(^1\Sigma_g^+) \leftarrow O_2(^3\Sigma_g^-)$ transitions. Our direct excitation experiment here had the advantage of being able to monitor the absorption of $O_2(^1\Sigma_g^+) \leftarrow O_2(^3\Sigma_g^-)$ via photoacoustic spectroscopy[6] simultaneously with the rate coefficient measurements to ensure tuning to the peak of the transition.

Tables 2−7 show our results as well as those from previous determinations of the rate coefficients for reactions 3−8. Generally speaking, our results are in good agreement with previous determinations. We note here again that, for most of these reactions, ours was the first study to observe the rate of formation of a product to determine the overall rate coefficient for the removal of $O_2(^1\Sigma_g^+)$. The individual rate coefficients are discussed below.

O_3. Our room-temperature value of k_3 is in excellent agreement with the previously recommended value,[10] which is based upon studies that employed both discharge[20] and flash photolytic[16,17,25,39,44,53,54] sources for the production of $O_2(^1\Sigma_g^+)$ (see Table 2). This rate coefficient is the easiest to measure

TABLE 2: Rate Coefficient Measurements for the Reaction $O_2(^1\Sigma_g^+) + O_3$

temp range (K)	room temp rate coeff (10^{-11} cm^3 molecule^{-1} s^{-1})	Arrhenius *A* factor (10^{-11} cm^3 molecule^{-1} s^{-1})	Arrhenius E_a/R (K)	reference
	2.5 ± 0.5			Gilpin et al., 1971[53]
	2.3 ± 0.5			Gauthier and Snelling, 1975[39]
	2.2 ± 0.2			Slanger and Black, 1979[17]
	1.8 ± 0.2			Amimoto and Weisenfeld, 1980[16]
295−362	2.2 ± 0.3	2.2 ± 0.3	0 ± 300	Choo and Leu, 1985[20]
	1.8 ± 0.3			Ogren et al., 1982[44]
	1.96 ± 0.03			Shi and Barker, 1990[25]
	$2.06 + 0.34$			Turnipseed et al., 1991[54]
	2.26 ± 0.30			Green et al., 2000[55]
295−362	**2.2 ± 0.8**	**2.2 ± 0.4**	**0 ± 200**	**JPL, 2000[10]**
210−370	**2.36 ± 0.26**	**3.63 ± 0.86**	**115 ± 66**	**this work, 2005**

TABLE 3: Rate Coefficient Measurements for the Reaction $O_2(^1\Sigma_g^+) + H_2O$

temp range (K)	room temp rate coeff (10^{-12} cm^3 molecule^{-1} s^{-1})	Arrhenius A factor (10^{-12} cm^3 molecule^{-1} s^{-1})	Arrhenius E_a/R (K)	reference
	3.3 ± 0.8			Filseth et al., 1970[36]
	4.0 ± 0.6			O'Brien and Myers, 1970[28]
	5.5 ± 2.8			Stuhl and Niki, 1970[38]
	4.67 ± 0.3			Derwent and Thrush, 1971[29]
	5.1 ± 2.1			Gautheir and Snelling, 1975[39]
	6.71 ± 0.53			Aviles et al., 1980[48]
	6.0 ± 0.3			Shi and Barker, 1990[25]
	5.4 ± 3.2			**JPL, 2000[10]**
250−370	**5.41 ± 0.78**	**4.52 ± 2.14**	**-89 ± 210**	**this work, 2005**

using the previously employed techniques because it is sufficiently rapid. The agreement of these methods with our direct laser excitation method is, thus, not surprising. In addition to the studies that detected the fluorescence from $O_2(^1\Sigma_g^+)$, Ogren et al.[44] measured the time-resolved concentration of O_3 following the flash photolysis of O_3, and used a chemical model to determine k_3. Green et al.[55] followed the temporal evolution of vibrationally excited O_3 following the pulsed laser photolysis of O_3/O_2 mixtures, and their value for k_3 is in excellent agreement with ours. We note that our result agrees well with that from Turnipseed et al.[54] who used the same PP−RF detection method for $O(^3P)$, but used the photolysis of O_3 at 193 nm in the presence of O_2 to produce $O_2(^1\Sigma_g^+)$.

Currently, k_3 is recommended to be independent of temperature, with $E_a/R = 0 \pm 200$,[10] based upon a single temperature dependent (295−360 K) study by Choo and Leu.[20] Our data show a slight temperature dependence, $E_a/R = (115 \pm 70)$ K, which is within the uncertainty of the recommendation, but distinctly not zero. We believe that our value of E_a/R is more precise than that of Choo and Leu because it is based on more data and covers a wider range of temperatures. Additionally, our O_3 concentrations cover a range 20 times larger than that of Choo and Leu and thus enabled more precise determination of k_3.

H_2O. One of the most likely sources of uncertainty in the reported value of k_4 is the uncertainty in the H_2O concentration. We measured the H_2O concentration using Lyman−α absorption; this method had been inter-compared with three other techniques,[22] therefore we are confident that the H_2O concentration was accurately determined. Several checks were performed to ensure the accuracy of our measured values of k_4. $O(^3P)$ temporal profiles recorded with a constant H_2O flow and the Lyman − α lamp alternatively turned on and off were identical, confirming that the Lyman-α radiation did not significantly dissociate H_2O, nor create any products that reacted with either $O_2(^1\Sigma_g^+)$ or $O(^3P)$. Varying the 762 nm laser fluence by a factor of 2 did not affect the observed $O(^3P)$ profiles, suggesting that secondary reactions of $O_2(^1\Sigma_g^+)$, such as reactions 9 or 10, were not significant. Last, the first-order rate coefficient for the loss of $O_2(^1\Sigma_g^+)$ measured by exciting several different rotational lines of the $O_2(^1\Sigma_g^+) \leftarrow O_2(^3\Sigma_g^-)$ transition (R7R7, R11R11, and R9Q10) were the same; this observation also confirms that our measured rate coefficients were for rotationally thermalized $O_2(^1\Sigma_g^+)$. (Note: a change in the first-order rate coefficient for the loss of $O_2(^1\Sigma_g^+)$ would have been seen only if the $O_2(^1\Sigma_g^+)$ was not rotationally thermalized and if the different rotational states of $O_2(^1\Sigma_g^+)$ reacted differently. Rotational thermalization is expected because $O_2(^1\Sigma_g^+)$ was allowed 40 or more collisions with the bath gas before being removed by the reactant under our typical experimental conditions.)

As a further check, k_4 was determined relative to k_3 via a Stern−Volmer analysis from the measured height of the $O(^3P)$ signal levels at a series of H_2O concentrations in the presence of a constant O_3 concentration. Fitting a line to a scatter plot of the inverse of the signal level vs the ratio of the concentrations of H_2O and O_3 gives a slope equal to the ratio of k_4 to k_3. The relative value for k_4 from this method agreed within a factor of 2 with the directly determined value. Better agreement was not expected because of the long-term instability in $O(^3P)$ detection over the course of many $O(^3P)$ temporal profiles measurements.

Overall, our room-temperature value of k_4 is in excellent agreement with the current recommendation,[10] which is based upon several previous studies[25,36,38] (see Table 3). Several other studies[28,29,39,48] are also in good agreement with this recommendation. Again, multiple sources of $O_2(^1\Sigma_g^+)$ were used in these previous studies, and now with our results, multiple methods for determining the rate coefficient. To our knowledge, ours is the first determination of the temperature dependence of k_4.

N_2. Our room-temperature value of k_5 is in excellent agreement with the current recommendation,[10] which is the average of several previous studies[20,25,27,36,37,42,46,49] (see Table 4). Several other studies that used less direct methods for determining k_5[12,28,34] are also consistent with the recommendation. Just as for O_3 and H_2O, there is agreement between studies employing different techniques and using different $O_2(^1\Sigma_g^+)$ sources. We found k_5 to show no significant temperature dependence, and our value for E_a/R of -37 ± 40 K agrees well with the current

TABLE 4: Rate Coefficient Measurements for the Reaction $O_2(^1\Sigma_g^+) + N_2$

temp range (K)	room temp rate coeff (10^{-15} cm^3 molecule^{-1} s^{-1})	Arrhenius A factor (10^{-15} cm^3 molecule^{-1} s^{-1})	Arrhenius E_a/R	reference
	2.3			Izod and Wayne, 1968[27]
	2.2			Stuhl and Weldge, 1969[37]
	1.8 ± 0.45			Filseth et al., 1970[36]
	2.0 ± 0.5			Noxon, 1970[12]
	3.0 ± 1.0			O′Brien and Myers, 1970[28]
	2.2 ± 0.1			Martin et al., 1976[46]
	1.7 ± 0.08			Chatha et al., 1979[34]
200−350	2.06 ± 0.61	1.7 (+1.3/−0.8)	-48 ± 120	Kohse-Hoinghaus and Stuhl, 1980[42]
	1.7 ± 0.1			Choo and Leu, 1985[20]
	2.2 ± 0.2			Wildt et al., 1988[49]
	2.32 ± 0.14			Shi and Barker, 1990[25]
200−350	**2.1 ± 0.8**	**2.1 ± 0.4**	**0 ± 200**	**JPL, 2000[10]**
210−370	**2.28 ± 0.25**	**2.03 ± 0.30**	**-37 ± 40**	**this work, 2005**

TABLE 5: Rate Coefficient Measurements for the Reaction $O_2(^1\Sigma_g^+) + CO_2$

room temp rate coeff (10^{-13} cm^3 molecule^{-1} s^{-1})	reference
4.4 ± 1.1	Filseth et al., 1970[36]
4.2 ± 0.3	Davidson et al., 1973[56]
4.53 ± 0.29	Aviles et al., 1980[48]
5.0 ± 0.3	Muller and Houston, 1981[57]
4.6 ± 0.5	Choo and Leu, 1985[20]
2.4 ± 0.4	Wildt et al., 1988[49]
4.0 ± 0.1	Shi and Barker, 1990[25]
4.4 ± 0.2	Hohmann et al., 1994[43]
4.2 ± 1.7	**JPL, 2000[10]**
3.39 ± 0.36	**this work, 2004**

TABLE 6: Rate Coefficient Measurements for the Reaction $O_2(^1\Sigma_g^+) + CH_4$

room temp rate coeff (10^{-14} cm^3 molecule^{-1} s^{-1})	reference
11 ± 5.5	Filseth et al., 1970[36]
7.3 ± 0.3	Davidson and Ogryzlo, 1974[31]
9.2 ± 6.6	Gauthier and Snelling, 1975[39]
9.62 ± 0.91	Kohse-Hoinghaus and Stuhl, 1980[42]
8.1 ± 1.0	Wildt et al., 1988[49]
10.8 ± 1.1	**this work, 2005**

recommendation based on a previous determination[42] for this value of -48 ± 120 K.

CO_2. The currently recommended value[10] for k_6 of $(4.2 \pm 1.7) \times 10^{-13}$ cm^3 molecule^{-1} s^{-1} is based on several studies.[20,25,36,48,49,56,57] The result of Hohmann et al.[43] is also in agreement with this recommended value (see Table 5). The range of values used in the current recommendation is (2.4−5.0) $\times 10^{-13}$ cm^3 molecule^{-1} s^{-1} and our value of $(3.39 \pm 0.36) \times 10^{-13}$ cm^3 molecule^{-1} s^{-1} falls within this range and agrees with the recommendation given the large uncertainty. We note however that it is approximately 25% lower than the recommendation and that our error bars do not overlap with most of the other previously reported values shown in Table 5. It appears that there are a number of results that cluster around a value of 4.5×10^{-13} cm^3 molecule^{-1} s^{-1} and a number of studies that are closer to 3.0×10^{-13} cm^3 molecule^{-1} s^{-1}, including several not included in the current recommendation.[12,28,39] There is no clear delineation between these two groups of studies; further studies may decipher the origin of these differences.

CH_4. Our room-temperature value of k_7 agrees with four of the previous studies[36,39,42,49] listed in Table 6. Our error bars do not overlap, however, with those of Davidson and Ogryzlo,[31] who determined their value for k_7 relative to their value for k_6. Although there is no obvious reason for this discrepancy, we note that they used a microwave discharge source for the production of $O_2(^1\Sigma_g^+)$ and did not include systematic uncertainties in their reported uncertainty. They admit these systematic uncertainties are difficult to assess. We also note that their measured rate coefficient for the reaction of $O_2(^1\Sigma_g^+)$ with ethane is ≥15% lower than other previous determinations, implying a possible systematic underestimation of their rate coefficients for reactions of $O_2(^1\Sigma_g^+)$ with aliphatic hydrocarbons.

TABLE 7: Rate Coefficient Measurements for the Reaction $O_2(^1\Sigma_g^+) + CO$

room temp rate coeff (10^{-15} cm^3 molecule^{-1} s^{-1})	reference
3.3	Stuhl and Weldge, 1969[37]
3 ± 1	Noxon, 1970[12]
4.3 ± 1.1	Filseth et al., 1970[36]
<12	Gauthier and Snelling, 1975[39]
4.5 ± 0.5	Choo and Leu, 1985[20]
3.74 ± 0.87	**this work, 2005**

CO. Our room-temperature value for k_8 of $(3.74 \pm 0.87) \times 10^{-15}$ agrees with the three previous determinations[12,36,37] and one upper limit measurement[39] listed in Table 7. We note that our value is the most precise determination to date. In addition, we have determined an upper limit for the yield of $O(^3P)$ from reaction 8a to be < 0.06. Independently, we measured an upper limit for the yield of CO_2 also from reaction 8a to be $< 1.2 \times 10^{-3}$. We conclude that the upper limit for the branching ratio of reaction 8a is $< 1.2 \times 10^{-3}$, meaning that CO quenches $O_2(^1\Sigma_g^+)$ on more than 99.8% of the collisions where $O_2(^1\Sigma_g^+)$ is removed. To our knowledge, there are no previous measurements of the branching ratios for this reaction with which to compare. The implications of this branching ratio for the atmosphere are discussed at the end of this article.

O_2. Our determination of an upper limit for k_{10} was not a primary objective of this study, but rather a byproduct of other rate coefficient determinations. As a result, our upper limit for k_{11} ($<1.5 \times 10^{-15}$ cm^3 molecule^{-1} s^{-1}) is much higher than the recommended value[10] of 3.9×10^{-17} cm^3 molecule^{-1} s^{-1}, which is based upon several previous studies[25,33,34,40,41,46,47] that were aimed at this specific rate coefficient. Thus, our result provides validation of, but does not improve upon, these previous measurements.

Overall Trend in $O_2(^1\Sigma_g^+)$ Rate Coefficients. Here we examine the trend in the magnitude of the rate coefficients measured in this study. For reactions that quench $O_2(^1\Sigma_g^+)$, the assumption is that $O_2(^1\Sigma_g^+)$ is deactivated to $O_2(^1\Delta_g)$ via electronic-to-vibrational energy transfer. For this spin-allowed transition, the quenching efficiency would be expected to depend exponentially on how closely the energy of the excited vibrational products matches that of the energy difference between $O_2(^1\Sigma_g^+)$ and $O_2(^1\Delta_g)$ (15.0 kcal mol^{-1}).[1] It has been

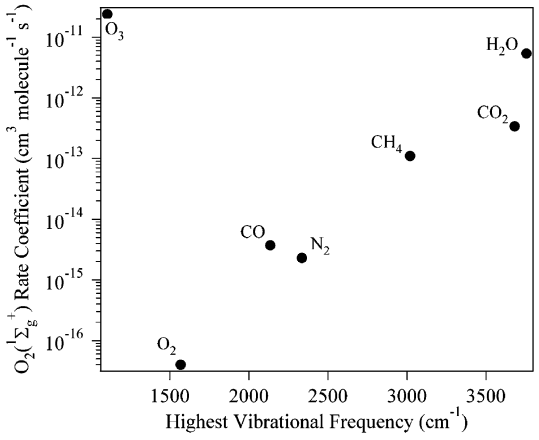

Figure 5. Plot of the $O_2(^1\Sigma_g^+)$ rate coefficient (on a log scale) vs the highest vibrational frequency of the reactant molecule. The expected log-linear trend is seen in general with the exception of O_3; see text for explanation.

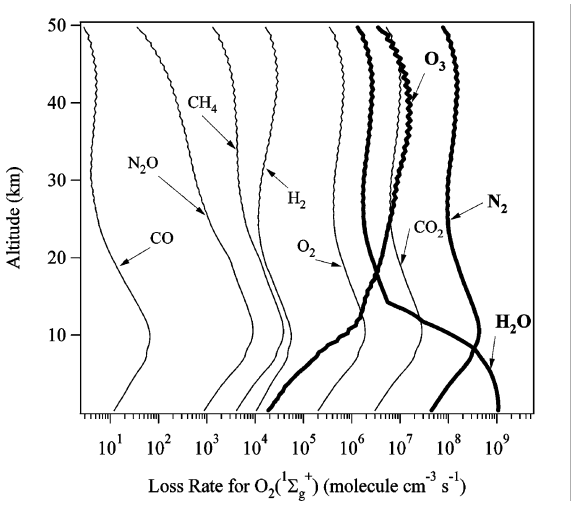

Figure 6. Atmospheric profiles for loss rates of $O_2(^1\Sigma_g^+)$ due to removal by various gas-phase species as determined from a simple box model employing the rate coefficients determined in this study. The major losses for $O_2(^1\Sigma_g^+)$ are due to removal by H_2O, N_2 and O_3.

stated more simply that the magnitude of the highest frequency vibration within the quencher determines the quenching efficiency; see Schweitzer and Schmidt[2] and references therein. We note that the review of Schweitzer and Schmidt includes a method for estimating the rate coefficient for the reaction of $O_2(^1\Sigma_g^+)$ with a polyatomic molecule by summing the contributions of individual bonds. For H_2O, this method yields a value within 10% of k_4 as measured here, and for CH_4, this method overestimates k_7 by a factor of more than 4, both of which are adequate given that the only available numbers are for the liquid phase and we are comparing to the gas phase. No information was available for O_3 as a reactant and this method does not provide much insight into the overall trend of the $O_2(^1\Sigma_g^+)$ rate coefficients measured here, so we return to the vibrational frequencies of the reactants.

We plot the $O_2(^1\Sigma_g^+)$ rate coefficients vs the highest ground state vibrational frequency in Figure 5. The expected log-linear trend is generally observed with the exception of reaction 3, that of $O_2(^1\Sigma_g^+)$ with O_3, which is 6 orders of magnitude larger than the trend would predict. We propose two possible explanations for why k_3 does not follow this trend and is the largest rate coefficient measured in this study. First, we note that $O_2(^1\Sigma_g^+)$ reaction with O_3 is the only reaction in this study that involves the formation of chemically different products, i.e., 2 O_2 + $O(^3P)$, with a branching ratio between 0.75 and 1.0.[16,17] For the first possible explanation, we note that 15.0 kcal mol^{-1} (0.65 eV) potentially released from the deactivation of $O_2(^1\Sigma_g^+)$ to $O_2(^1\Delta_g)$ is not sufficient energy to dissociate O_3 to $O(^3P)$ + $O_2(^3\Sigma_g^-)$ (~1.1 eV).[58,59] However, deactivation of $O_2(^1\Sigma_g^+)$ to $O_2(^3\Sigma_g^-)$ releases 37.5 kcal mol^{-1} (1.68 eV), which is more than the energy required to raise O_3 from its ground ($^1A_1$) state to one of four low lying electronic states: $^3A_2$, $^3B_2$, $^3B_1$, or $^1A_2$.[59,60] Three of these electronically excited states ($^3A_2$, $^3B_2$, and $^1A_2$) are adiabatically correlated to $O(^3P)$ and $O_2(^3\Sigma_g^-)$, and the fourth ($^3B_1$) is correlated to $O(^3P)$ and $O_2(^1\Delta_g)$. The transition of $O_2(^1\Sigma_g^+) \rightarrow O_2(^3\Sigma_g^-)$ is spin forbidden, and therefore may be expected to be inefficient, unless, however, complex formation enhances energy transfer. Thus, one explanation for why k_3 is relatively larger than the other $O_2(^1\Sigma_g^+)$ rate coefficients would be a relatively close match of the energy released in $O_2(^1\Sigma_g^+) \rightarrow O_2(^3\Sigma_g^-)$ deactivation to that gained by $O_3(^1A_1)$ excitation to one of the four possible low lying electronically excited states, involving complex formation followed by dissociation of the excited O_3 molecule to $O(^3P)$ and $O_2(^1\Sigma_g^+)$. The other possible explanation for the large magnitude of k_3 is an insertion of $O_2(^1\Sigma_g^+)$, into one of the bonds in O_3, followed by dissociation to form 2 O_2 + $O(^3P)$. Overall, it is clear that this reaction is complicated given that it proceeds via both quenching and reaction channels. Future experiments using isotopically labeled $O_2(^1\Sigma_g^+)$, crossed molecular beam studies, or high-pressure studies may be helpful in elucidating the exact mechanism.

Atmospheric Implications. The atmospheric implications of these findings were explored using a simple box model[22] to calculate the altitude dependent loss rates of $O_2(^1\Sigma_g^+)$. Atmospheric profiles of temperature, pressure, and chemical species were taken from the US Standard Atmosphere.[61] The $O_2(^1\Sigma_g^+)$ production rate was calculated using the *g*-factors from Mlynczak[62] and the tropospheric ultraviolet−visible radiation model developed at NCAR[8] (summed from 200 to 400 nm for O_3 photolysis with 1 nm wide bins centered on the integer wavelengths). The extraterrestrial flux from the Susium/Neckel satellite[8] for northern hemisphere spring equinox was used. No aerosols were incorporated, and the albedo was set at 5%. $O(^1D)$ quantum yields from O_3 photolysis were from Talukdar et al.[63] The temperature dependence for reaction 6 was taken from the measurement of Borrell et al.[51] We solved for the steady-state concentrations of $O_2(^1\Sigma_g^+)$ and its loss rate as a function of altitude.

Figure 6 shows the atmospheric loss rates of $O_2(^1\Sigma_g^+)$; the lifetime of $O_2(^1\Sigma_g^+)$ in the troposphere is on the order of 10^{-5} s, while the lower stratospheric lifetime is longer, on the order of 10^{-3} s. We can compare this to the radiative lifetime of $O_2(^1\Sigma_g^+)$ of 11.3 s. Thus, the majority of $O_2(^1\Sigma_g^+)$ is quenched in the atmosphere. The major quenchers of $O_2(^1\Sigma_g^+)$ are H_2O and N_2 in the troposphere, and N_2, CO_2 and O_3 at altitudes above that. It is interesting to note that at no altitude does O_2 itself contribute significantly to the removal of $O_2(^1\Sigma_g^+)$.

Additionally, we employed this box model to show the relative effect of reaction 8a as a potential sink for CO. We determined the loss rate of CO using our upper limit for reaction 8a and a standard profile of atmospheric CO. The CO loss rate due to reaction with $O_2(^1\Sigma_g^+)$ contributes at most 0.02% to the loss of CO, where the majority of CO is lost via the reaction with OH.[10,64] In addition, we note that the CO_2 production rate from reaction 8a was less than 0.1 molecules cm^{-3} s^{-1} at all altitudes up to 50 km, which is negligible. In conclusion, reaction

8a is a negligible process for both CO loss and CO_2 production in the atmosphere.

Acknowledgment. We gratefully acknowledge John Daniel and Gregory Frost for their assistance in the modeling work. This work was funded in part by NOAA's Climate Change program, in part by NASA's Upper Atmospheric Research Program and in part by NASA's Earth System Science Doctoral Fellowship to E.J.D. These results are also presented as a part of E.J.D.'s Ph.D. thesis.

References and Notes

(1) Wayne, R. P. Reactions of sinlget molecular oxygen in the gas phase. In *Singlet O_2, Vol. 1, Physical-chemical aspects*; Frimer, A. A., Ed.; CRC Press: Boca Raton, FL, 1985; pp 81−172.
(2) Schweitzer, C.; Schmidt, R. *Chem. Rev.* **2003**, *103*, 1685−1757.
(3) Toumi, R. *Geophys. Res. Lett.* **1993**, *20*, 25−28.
(4) Siskind, D. E.; Summers, M. E.; Mlynczak, M. G. *Geophys. Res. Lett.* **1993**, *20*, 2047−2050.
(5) Prasad, S. S. *J. Geophys. Res.* **1997**, *102*, 21, 527−521, 536.
(6) Talukdar, R. K.; Dunlea, E. J.; Brown, S. B.; Daniel, J. S.; Ravishankara, A. R. *J. Phys. Chem.* **2002**, *106*, 8461−8470.
(7) Dunlea, E. J.; Talukdar, R. K.; Ravishankara, A. R. To be submitted for publication.
(8) Madronich, S.; Zeng, J.; Stamnes, K. Tropospheric ultraviolet−visible radiation model; Version 3.8 ed., 1997.
(9) Rothman, L. S.; Rinsland, C. P.; Goldman, A.; Massie, S. T.; Edwards, D. P.; Flaud, J. M.; Perrin, A.; Camy-Peyret, C.; Dana, V.; Mandin, J. Y.; Schroeder, J.; McCann, A.; Gamache, R. R.; Watson, R. B.; Yoshino, K.; Chance, K. V.; Jucks, K. W.; Brown, L. R.; Nemtchinov, V.; Varanasi, R. *J. Quant. Spectros. Radiat. Transfer* **1998**, *60*, 665−710.
(10) Sander, S. P.; Golden, D. M.; Hampson, R. F.; Kurylo, M. J.; Howard, C. J.; Ravishankara, A. R.; Kolb, C. E.; Molina, M. J. *Chemical kinetics and photochemical data for use in stratospheric modeling*; Jet Propulsion Laboratory, California Insitute of Technology: Pasadena, CA, 2000.
(11) Lee, L. C.; Slanger, T. G. *J. Chem. Phys.* **1978**, *69*, 4053−4060.
(12) Noxon, J. F. *J. Chem. Phys.* **1970**, *52*, 1852−1873.
(13) Snelling, D. R. *Can. J. Chem.* **1974**, *52*, 257−270.
(14) Biedenkapp, D.; Bair, E. J. *J. Chem. Phys.* **1970**, *52*, 6119−6125.
(15) Dunlea, E. J.; Ravishankara, A. R. *Phys. Chem. Chem. Phys.* **2004**, *6*, 2152−2161.
(16) Amimoto, S. T.; Wiesenfeld, J. R. *J. Chem. Phys.* **1980**, *72*, 3899−3903.
(17) Slanger, T. G.; Black, G. *J. Chem. Phys.* **1979**, *70*, 3434−3438.
(18) Wine, P. H.; Ravishankara, A. R. *Chem. Phys. Lett.* **1981**, *77*, 103−109.
(19) Warren, R. F.; Ravishankara, A. R. *Int. J. Chem. Kinet.* **1993**, *25*, 833−844.
(20) Choo, K. Y.; Leu, M.-T. *Int. J. Chem. Kinet.* **1985**, *17*, 1155−1167.
(21) Tsang, W.; Hampson, R. F. *J. Phys. Chem. Ref. Data* **1986**, *15*, 1087.
(22) Dunlea, E. J.; Ravishankara, A. R. *Phys. Chem. Chem. Phys.* **2004**, *6*, 3333−3340.
(23) Kley, D. *J. Atmos. Chem.* **1984**, *2*, 203−210.
(24) Vatsa, R. K.; Volpp, H.-R. *Chem. Phys. Lett.* **2001**, *340*, 289−295.
(25) Shi, J.; Barker, J. R. *Int. J. Chem. Kinet.* **1990**, *20*, 1283−1301.
(26) Calvert, J. G.; Pitts, J. N. *Photochemistry*; John Wiley & Sons: New York, 1966.
(27) Izod, T. P. J.; Wayne, R. P. *Proc. R. Soc. A* **1968**, *308*, 81−94.
(28) O'Brien, R. J., Jr.; Myers, G. H. *J. Chem. Phys.* **1970**, *53*, 3832−3835.
(29) Derwent, R. G.; Thrush, B. A. *Trans. Faraday Soc.* **1971**, *67*, 2036−2043.
(30) Becker, K. H.; Groth, W.; Schurath, U. *Chem. Phys. Lett.* **1971**, *8*, 259−262.
(31) Davidson, J. A.; Ogryzlo, E. A. *Can. J. Chem.* **1974**, *52*, 240−245.
(32) Thomas, R. G. O.; Thrush, B. A. *J. Chem. Soc., Faraday Trans. 2* **1975**, *71*, 664−667.
(33) Thomas, R. G. O.; Thrush, B. A. *Proc. R. Soc. A* **1977**, *356*, 287−294.
(34) Chatha, J. P. S.; Arora, P. K.; Raja, N.; Kulkarni, P. B.; Vohra, K. G. *Int. J. Chem. Kinet.* **1979**, *11*, 175−185.
(35) Singh, J. P.; Setser, D. W. *J. Phys. Chem.* **1985**, *89*, 5353−5358.
(36) Filseth, S. V.; Zia, A.; Welge, K. H. *J. Chem. Phys.* **1970**, *52*, 5502−5510.
(37) Stuhl, F.; Welge, K. H. *Can. J. Chem.* **1969**, *47*, 1870−1871.
(38) Stuhl, F.; Niki, H. *Chem. Phys. Lett.* **1970**, *7*, 473−474.
(39) Gauthier, M. J. E.; Snelling, D. R. *J. Photochem.* **1975**, *4*, 27−50.
(40) Lawton, S. A.; Novick, S. E.; Broida, H. P.; Phelps, A. V. *J. Chem. Phys.* **1977**, *66*, 1381−1382.
(41) Lawton, S. A.; Phelps, A. V. *J. Chem. Phys.* **1978**, *69*, 1055−1068.
(42) Kohse-Höinghaus, K.; Stuhl, F. *J. Chem. Phys.* **1980**, *72*, 3720−3726.
(43) Hohmann, J.; Muller, G.; Schonnenbeck, G.; Stuhl, F. *Chem. Phys. Lett.* **1994**, *217*, 577−581.
(44) Ogren, P. J.; Sworski, T. J.; Hochanadel, C. J.; Cassel, J. M. *J. Phys. Chem.* **1982**, *86*, 238−242.
(45) Slanger, T. G.; Lee, L. C. *J. Chem. Phys.* **1978**, *69*, 4053−4060.
(46) Martin, L. R.; Cohen, R. B.; Schatz, J. F. *Chem. Phys. Lett.* **1976**, *41*, 394−396.
(47) Knickelbein, M. B.; Marsh, K. L.; Ulrich, O. E.; Busch, G. E. *J. Chem. Phys.* **1987**, *87*, 2392−2393.
(48) Aviles, R. G.; Muller, D. F.; Houston, P. L. *Appl. Phys. Lett.* **1980**, *37*, 358−360.
(49) Wildt, J.; Bednarek, G.; Fink, E. H.; Wayne, R. P. *Chem. Phys.* **1988**, *122*, 463−470.
(50) Boodaghians, R. B.; Borrell, P. M.; Borrell, P. *Chem. Phys. Lett.* **1983**, *97*, 193−197.
(51) Borrell, P. M.; Borrell, P.; Grant, K. R. *J. Chem. Phys.* **1983**, *78*, 748−756.
(52) Borrell, P.; Richards, D. S. *J. Chem. Soc., Faraday Trans. 2* **1989**, *85*, 1401−1411.
(53) Gilpin, R.; Schiff, H. I.; Welge, K. H. *J. Chem. Phys.* **1971**, *55*, 1087−1093.
(54) Turnipseed, A. A.; Vaghjiani, G. L.; Gierczak, T.; Thompson, J. E.; Ravishankara, A. R. *J. Chem. Phys.* **1991**, *95*, 3244−3251.
(55) Green, J. G.; Shi, J.; Barker, J. R. *J. Phys. Chem. A* **2000**, *104*, 6218−6226.
(56) Davidson, J. A.; Kear, K. E.; Abrahamson, E. W. *J. Photochem.* **1972/3**, *1*, 307−316.
(57) Muller, D. F.; Houston, P. L. *J. Phys. Chem.* **1981**, *85*, 3563−3565.
(58) Hay, P. J.; Dunning, T. H. *J. Chem. Phys.* **1977**, *67*, 2290−2303.
(59) Arnold, D. W.; Xu, C.; Kim, E. H.; Neumark, D. M. *J. Chem. Phys.* **1994**, *101*, 912−922.
(60) Swanson, N.; Celotta, R. J. *Phys. Rev. Lett.* **1975**, *35*, 783−785.
(61) *U. S. Standard Atmosphere*; U.S. Government Printing Office, Washington, DC, 1976.
(62) Mlynczak, M. G. *Geophys. Res. Lett.* **1993**, *20*, 1439−1442.
(63) Talukdar, R. K.; Longfellow, C. A.; Gilles, M. K.; Ravishankara, A. R. *Geophys. Res. Lett.* **1998**, *25*, 143−146.
(64) McCabe, D. C.; Gierczak, T.; Talukdar, R. K.; Ravishankara, A. R. *Geophys. Res. Lett.* **2001**, *28*, 3135−3138.